

Multi-defect microscopy image restoration under limited data conditions

Anastasia Razdaibiedina

Vector Institute
University of Toronto
anastasia.razdaibiedina@mail.utoronto.ca

Jeevaa Velayutham

University of Toronto
jevaav@cs.toronto.edu

Miti Modi

University of Toronto
miti.modi@mail.utoronto.ca

Abstract

Deep learning methods are becoming widely used for restoration of defects associated with fluorescence microscopy imaging. One of the major challenges in application of such methods is the availability of training data. In this work, we propose a unified method for reconstruction of multi-defect fluorescence microscopy images when training data is limited. Our approach consists of two steps: first, we perform data augmentation using a Generative Adversarial Network (GAN) with conditional instance normalization (CIN); second, we train a conditional GAN (cGAN) on paired ground-truth and defected images to perform the restoration. The experiments on three common types of imaging defects with different amounts of training data, show that the proposed method gives comparable results or outperforms CARE, deblurGAN and CycleGAN in restored image quality when limited data is available.

1 Introduction

Degradation of fluorescence microscopy images occurs due to many factors, including bleaching of fluorophores, readout noise from sensors, out-of-focus light, poor axial sampling, and uneven illumination and detection [1]. Microscopy hardware constraints and physical limitations often make it impossible to simultaneously overcome multiple types of imaging defects. Hence, the application of image reconstruction pipelines is becoming increasingly popular. In this work we focus on three common tasks in microscopy image restoration: *denoising*, *axial inpainting*, and deep learning enabled *super-resolution* [1, 2, 3].

We used three publicly available datasets, which represent the above-mentioned defect types (Table 1) [4]. For image quality assessment, we used Peak Signal-to-Noise Ratio (PSNR) and Structural Similarity index (SSIM) scores [5].

Organism	Biological Structure	Restoration task	average PSNR / SSIM
Drosophila	whole embryo	denoising	19.92 / 0.63
Zebrafish	retinal nuclei	axial inpainting	12.51 / 0.33
Human	HeLa cells microtubules	super-resolving	7.27 / 0.08

Table 1: Description of datasets used for the experiments. PSNR / SSIM column denotes average PSNR and SSIM scores across the whole dataset before image reconstruction.

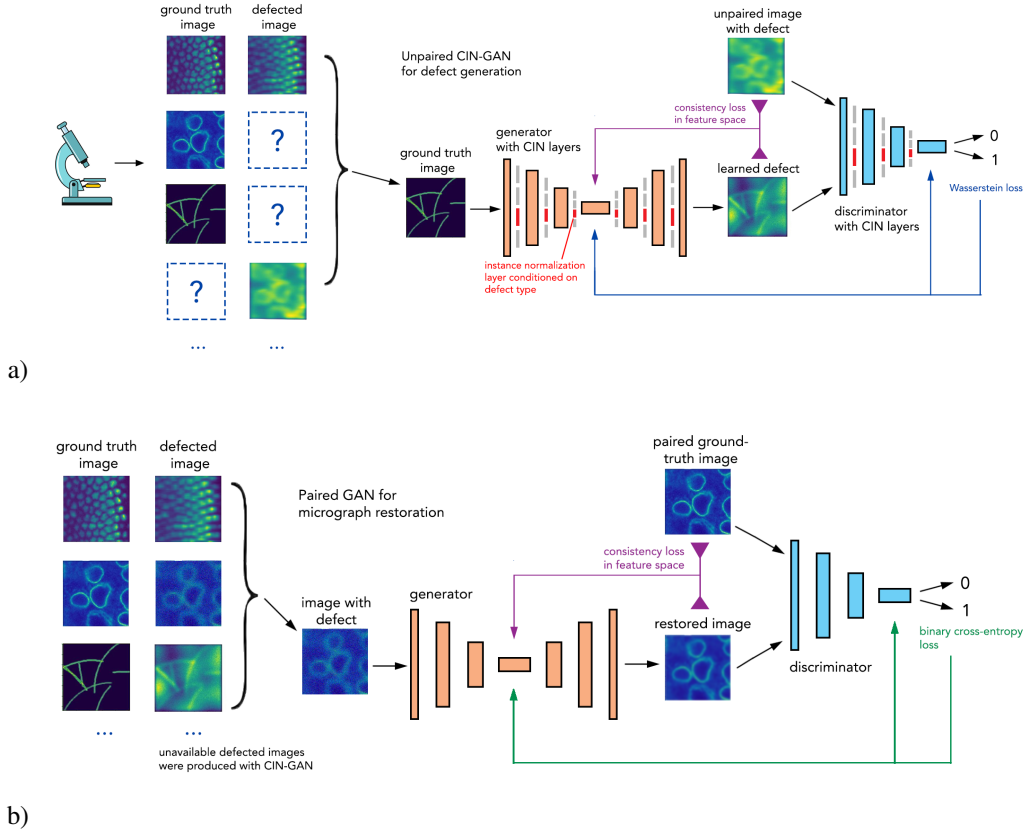


Figure 1: Illustration of the proposed pipeline. a) GAN with conditional instance normalization (CIN) layers for generating different microscopy defects. Since paired data is often unavailable, CIN-GAN is trained on a small amount of unpaired defected and ground truth microscopy image data; different CIN layers are "switched" on / off depending on the task. b) Conditional GAN for image restoration. This GAN is trained on paired data, where the previously unavailable defected image pairs are now produced by CIN-GAN.

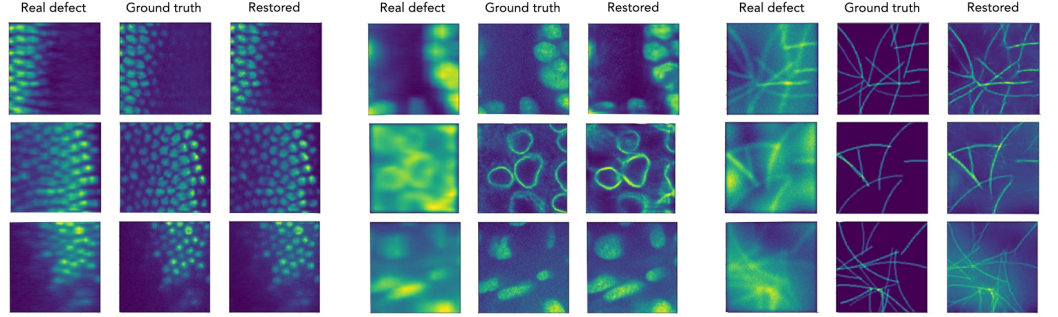
Considering the diversity of reconstruction tasks in fluorescent microscopy, and due to an increasing need in data-driven image restoration approaches, we propose a unified method for multi-defect micrograph restoration. To overcome the problem of limited training data, which is a common challenge for experimental databases, we incorporate meta-learning style data augmentation into our pipeline.

2 Method

The proposed pipeline consists of two GANs [6]. First, a GAN with CIN layers is trained to perform data augmentation using limited amount of unpaired ground-truth and defected images. We apply condition on the instance normalization for each defect type as proposed by [7]:

$$z = \gamma_i \left(\frac{x - \mu}{\sigma} \right) + \beta_i \quad (1)$$

where i is the number of tasks, μ and σ are mean and standard deviation respectively of the input. The parameters γ_i and β_i are learned separately for each task. Thus, all other layers in the model are shared across tasks, except for the instance normalization layers that drive distinct defects synthesis. Second, the dataset is augmented by CIN-GAN and a cGAN [8] is trained on paired high-resolution ground-truth images and defective images. The resulting cGAN is used to restore multiple types of microscopy defects. For training of both GANs we used adversarial and content losses, where



(a) Denoising of Drosophila embryonic cells. (b) Axial inpainting of Zebrafish retinal nuclei. (c) Super-resolving microtubules of HeLa cells.

Figure 2: Examples of micrographs restoration with the proposed pipeline on three distinct tasks. 10 real pairs of images were used for training; dataset was augmented with CIN-GAN.

content loss measures image consistency in feature space of VGG16 model [9, 10]:

$$L_{total} = L_{adv} + \lambda \cdot L_{content} \quad (2)$$

3 Results

We compared performance of our restoration pipeline in two settings: A) a limited amount of real paired images (defected + in-focus) are available; B) no real pairs are available, all defected pairs for cGAN training were synthetically generated. Restoration results under setting of 10 paired images are shown in Figure 2.

A) For the paired setting, we compared our model performance with two existing state-of-the-art image restoration models: (1) DeblurGAN [11], (2) U-Net based [12] CARE models [4]. These two models are trained on paired images, that is, we assume that there are real paired images available for model training. We outperformed both models for most tasks from 10 to 50 pairs of images, results for 10 pairs of images are shown in Table 2 and Figure 2. B) For the unpaired setting we assumed that real paired training data was not available. CIN-GAN was used to generate artificial defects to create paired training data for cGAN which restores the real defected images. We compare this performance with state-of-the-art unpaired image to image translation model, CycleGAN [13] in Table 2.

We have also shown advantage of using CIN-GAN in the limited data setting by comparing performance of data augmentation via CIN-GAN and separately trained GANs (Figure 3).

	Denoising	Axial inpainting	Super-resolution
CARE	21.6/ 0.56	12.8/0.29	14.1/0.20
DeblurGAN	18.0/0.33	14.6/0.20	11.2/0.14
Ours	22.4/0.56	17.4/0.38	14.3/0.22
CycleGAN	21.3/0.49	15.3/0.27	12.7/0.14
Ours	21.9/0.57	15.1/ 0.32	8.9/0.07

Table 2: Comparison of PSNR/SSIM scores between our cGAN restoration network with other models with 10 paired images (top) or no paired data (bottom).

Thus, we proposed a unified method for microscopy image restoration that is applicable for reconstruction of multiple defect types under limited data conditions. With the help of GAN-based data augmentation we are able to overcome the problem of unpaired limited data. The proposed pipeline achieves competitive results on three microscopy databases and can be scaled up to more defect types.

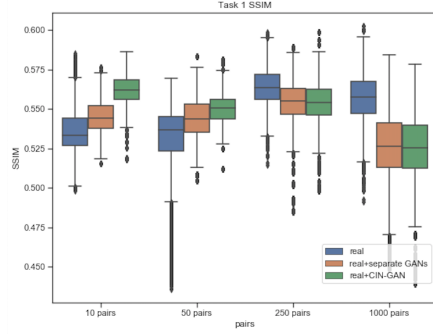


Figure 3: Benefit of GAN-based data augmentation. Boxplots show the distribution of SSIM scores for restored images for real paired data, real data augmented by separate GANs and real data augmented by CIN-GAN. Plots are shown for 10, 50, 250 and 1000 data pairs. CIN-GAN data augmentation proves to be beneficial in cases when limited paired data is available.

References

- [1] C. Belthangady and L. A. Royer, “Applications, promises, and pitfalls of deep learning for fluorescence image reconstruction,” *Nature methods*, p. 1, 2019.
- [2] F. Luisier, T. Blu, and M. Unser, “Image denoising in mixed poisson–gaussian noise,” *IEEE Transactions on image processing*, vol. 20, no. 3, pp. 696–708, 2010.
- [3] L. Schermelleh, A. Ferrand, T. Huser, C. Eggeling, M. Sauer, O. Biehlmaier, and G. P. Drummen, “Super-resolution microscopy demystified,” *Nature cell biology*, vol. 21, no. 1, p. 72, 2019.
- [4] M. Weigert, U. Schmidt, T. Boothe, A. Müller, A. Distrov, A. Jain, B. Wilhelm, D. Schmidt, C. Broadus, S. Culley, M. Rocha-Martins, F. Segovia-Miranda, C. Norden, R. Henriques, M. Zerial, M. Solimena, J. Rink, P. Tomančák, L. A. Royer, F. Jug, and E. W. Myers, “Content-aware image restoration: pushing the limits of fluorescence microscopy,” *Nature Methods*, vol. 15, pp. 1090–1097, 2018.
- [5] J. Wang, A. C. Bovik, H. R. Sheikh, and E. P. Simoncelli, “Image quality assessment: from error visibility to structural similarity,” *IEEE Transactions on Image Processing*, vol. 13, pp. 600–612, 2004.
- [6] I. J. Goodfellow, J. Pouget-Abadie, M. Mirza, B. Xu, D. Warde-Farley, S. Ozair, A. C. Courville, and Y. Bengio, “Generative adversarial nets,” in *NIPS*, 2014.
- [7] V. Dumoulin, J. Shlens, and M. Kudlur, “A learned representation for artistic style,” *CoRR*, vol. abs/1610.07629, 2017.
- [8] P. Isola, J.-Y. Zhu, T. Zhou, and A. A. Efros, “Image-to-image translation with conditional adversarial networks,” in *Proceedings of the IEEE conference on computer vision and pattern recognition*, pp. 1125–1134, 2017.
- [9] L. A. Gatys, A. S. Ecker, and M. Bethge, “A neural algorithm of artistic style,” *CoRR*, vol. abs/1508.06576, 2015.
- [10] K. Simonyan and A. Zisserman, “Very deep convolutional networks for large-scale image recognition,” *arXiv preprint arXiv:1409.1556*, 2014.
- [11] O. Kupyn, V. Budzan, M. Mykhailych, D. Mishkin, and J. Matas, “Deblurgan: Blind motion deblurring using conditional adversarial networks,” *2018 IEEE/CVF Conference on Computer Vision and Pattern Recognition*, pp. 8183–8192, 2018.
- [12] O. Ronneberger, P. Fischer, and T. Brox, “U-net: Convolutional networks for biomedical image segmentation,” in *International Conference on Medical image computing and computer-assisted intervention*, pp. 234–241, Springer, 2015.
- [13] J.-Y. Zhu, T. Park, P. Isola, and A. A. Efros, “Unpaired image-to-image translation using cycle-consistent adversarial networks,” *2017 IEEE International Conference on Computer Vision (ICCV)*, pp. 2242–2251, 2017.